On the coupling of the Biot model with reactive transport

by
Oda Gilhuus Gregusson

Master of Science Thesis in
Applied and Computational Mathematics

Department of Mathematics
University of Bergen

June 2019

Acknowledgements

First, I would like to thank my supervisors Professor Adrian Florin Radu and Mats Kirkesæther Brun for their guidance. I give my thanks to Florin for suggesting the topic, and for sharing his knowledge and thoughts, and to Mats for his computational skills and for always replying to all my e-mails within short time, even the day before Christmas.

I would also like to thank Erlend Storvik for his availability and our good conversations. To all my good friends, my boyfriend, my mother, thanks for always being supportive and making me laugh even on my worst days. Finally, thank you Hannah for all your motivational quotes.

Abstract

In this thesis, we study the iterative solution of coupled flow, mechanics and transport in deformable porous media. The system is modeled by the quasi-static Biot equations and the advection-diffusion-reaction equation. This model is analyzed numerically by using a variation of the well-known Fixed Stress Splitting method. The spatial discretization employed is piecewise linear Galerkin finite elements for mechanics and transport, and lowest order Raviart-Thomas elements for flow. Additionally, the backward Euler method is employed for the time discretization. Three different alternatives for the stabilization constant introduced by the fixed stress splitting scheme are analyzed, and the optimal choice for this constant is found. The scheme is also analyzed with and without the stabilization terms introduced by linearization of the reaction term in the transport equation, and the result is that this has no impact on the iteration count for the scheme. Moreover, four different reaction terms are studied, and the result is that they are all convergent. We also study the efficiency of the fixed stress splitting scheme by comparing it with two different monolithic schemes. One where only the Biot equations are solved monolithically, and one were the whole system is solved monolithically. The conclusion is that the fixed stress splitting scheme is the most efficient method for solving our system of equations for finer meshes. For coarser meshes, the choice of method is of little consequence. Furthermore, two different domains are studied, the unit square and the L-shaped domain. Performing convergence tests on the system, give results that are consistent with the optimal theoretical convergence rates for both domains.

Contents

Chapter 1

Introduction

1.1 Introduction

Porous media is found everywhere around us. In the sand on the beach we walk on, the sponge we clear the blackboard with, the ground beneath us, and even inside our bodies. It is defined as a material containing pores and a solid skeleton. To describe the porous media, a partial differential equation is required. In realistic models, the equations can be problematic to solve analytically, in which case a numerical method is needed. An example of a realistic application of the theory of porous media concerns the modeling of a tumor. The tumor can be viewed as a deformable porous medium with a fluid flow that may cause, or be affected by, solid deformation. Furthermore, the fluid flow can be coupled with the transport of a substance of interest. This substance can for example be oxygen or a growth stopping medicament.

For this thesis, we will consider the quasi-static Biot equations coupled with the transport equation. The quasi-static Biot equations models a linearly elastic porous medium saturated with a slightly compressible fluid, and have previously been used to partly describe tumor growth (Xue et al., 2016). The equations are based on the balance of momentum, mass conservation and Darcy's law, with application to infinitesimally deforming, fully saturated porous media. The existence, uniqueness, and regularity of the Biot equations was studied in Showalter (2000).

There are two approaches that accurately solves numerically coupled flow and mechanics. One approach is a monolithic scheme, where the equations are fully coupled and solved simultaneously, achieving unconditional stability and convergence for well-posed problems. The other approach is a sequential implicit method. Here, the coupled problem is partitioned into sub-problems (i.e. flow and mechanics) that are solved sequentially, usually by an already existing, robust simulator, which causes this approach to be more flexible and less computationally expensive (Settari and Mourits, 1998).
Among these sequential implicit methods, the Fixed Stress Splitting method stands out as the optimal choice for the quasi-static Biot equations (Kim et al., 2011). This method is unconditionally stable by Von Neumann analysis (Kim et al., 2009) and globally convergent (Mikelić and Wheeler, 2013) for slightly compressible flow in heterogeneous porous media (Both et al., 2017). It is an iterative method that fixes the total mean stress field by introducing a tuning parameter when the sub-problem for the flow is solved. The sub-problem for the mechanics is then solved using the computed pressure from the previously solved flow sub-problem. This process is iterated until convergence is reached.

We want to couple the Biot equations with the transport equation in order to further advance the model to include transport of a substance. This is an important step in order to create a more realistic model that in the future may be used for modeling tumor growth.
The transport equation we will consider is an advection-diffusion-reaction equation which models how a substance is transferred within the fluid. The advection describes the movement of the substance within the medium by transportation of the flow field, the diffusion describes the movement of the substance from an area of high concentration to an area of low concentration, and the reaction describes the creation or destruction of the substance as a reaction to itself. This equation will be coupled with the Biot equations in the sense that the flow field used in the transport equation will be the Darcy flux from the approximated solution of the Biot equations.
To avoid influence by steep concentration gradients in the transport equation, which happens if the equation is advection-dominant, we need the employed numerical method to have minimal oscillation and numerical diffusion. In Kim et al. (2009) it

was shown that this was indeed the case for the fixed stress splitting method, hence this will follow when coupling the Biot equations with the transport equation, as the concentration does not have any impact on the pressure or displacement. The transport equation is linearized and stabilized by the use of the L-scheme, such as in e.g. (List and Radu, 2016), (Borregales et al., 2018), (Brun et al., 2019).

For discretization of the Biot equations, we consider a mixed formulation for the mass conservation equation, which provides an accurate Darcy velocity and a flow approximation that is locally mass conservative when discretizing using the finite element method. The Biot equations and the transport equation is then discretized by using a finite element method. To simplify the presentation, we consider a fixed time domain and the unit square. Following this we consider an L-shaped domain, limited on the outer edges by the unit square.

Furthermore, we want to study different tuning parameters for the fixed stress splitting scheme on both domains to find the optimal choice. The stabilization terms introduced by linearization of the reaction term in the transport equation are also studied. Moreover, different reaction terms for the transport equation are analyzed. The efficiency of the fixed stress splitting scheme is examined by comparing the time elapsed for this scheme with the time elapsed for two different monolithic schemes. Lastly, the convergence rates of our numerical schemes are analyzed in order to validate our model.

The analysis in this thesis is presented for fully saturated flow and nonlinear transport. An extension to unsaturated flow can be studied following the approach developed in Both et al. (2019).

1.2 Outline

Chapter 2 and 3 introduces the basic concepts, equations and ideas used in this thesis. Specifically, in Section 2.1 the Darcy law is explained in detail, while in Section 2.2 the mass conservation law is derived and is connected to the Darcy law. Moreover, in Section 2.3 the transport equation is presented and explained, and in Section 2.4 the Biot equations are introduced and explained in detail. Furthermore,

in Section 3.1 discretization in time is explained in detail, and in Section 3.2 the finite element method is made clear. Finally, in Section 3.3 an iterative scheme is explained in general, and the iterative schemes usually employed when modeling flow in porous media are presented and discussed.

Section 3.4 presents the assumptions made on our model and extends the previously presented concepts and ideas to the Biot equations and transport equation. Moreover, a fixed stress splitting iterative scheme is presented for our model.

In Chapter 4, the problem data is accounted for, the numerical results are presented and an analysis on the data is performed and presented.

Finally, in Chapter 5.1 the conclusion and further work is discussed.

Chapter 2

Mathematical Modeling

In this thesis we consider a fully saturated elastic porous medium. To get a better understanding of the relevant mathematical models, we first explain the definition of a porous medium.

A porous medium is defined as a material containing pores and a solid skeleton, which in our case is deformable. The porous media should have a specific permeability, whose value is uniquely determined by the pore geometry (Dullien, 1979). The permeability of a porous medium is defined as a measure of how easily a fluid can flow through the medium. For a fluid to be able to flow through the media, the pores have to be interconnected (Pettersen, 1990). An example of how a porous media can present itself is given in Figure 2.1.

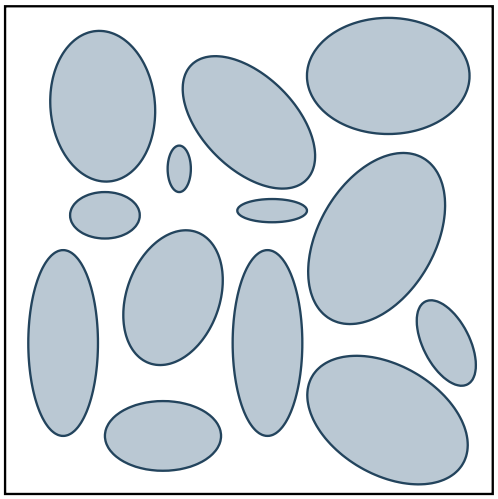

Figure 2.1: An example of a porous media with grey parts being the solid grains, i.e. the solid skeleton, and the white part being the pores.

The phase of the porous medium depends on the number of fluids present in the pores. If there is only one fluid, the porous medium is defined as single-phase, while if there are two or several fluids present, it is defined as two-phase or multi-phase, respectively (Bear, 1988). The fluid can be either a gas or a liquid, for instance oxygen or water. Some examples of deformable porous media are sponges, sand and tumors.

To simplify the calculations of porous media, a representative elementary volume method, i.e. a REV method, is often used to define the local properties of a porous medium. This method is a smoothing procedure where you give one mathematical point in space the properties of a certain volume, the REV, of material surrounding this point. The reason for using this method is that porosity and permeability cannot be defined or measured at single points, considering that a porous medium is a collection of solid grains and voids. When deciding the size of the REV, it has to be large enough to contain a substantial number of pores, so that we can find a mean global property, but also small enough so that we can approximate the parameter variations by continuous functions (Bear, 1988).

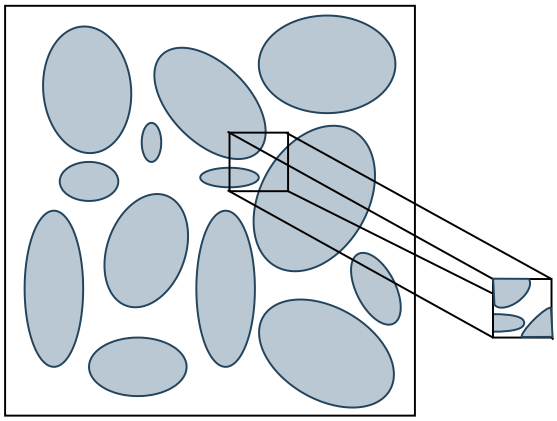

Figure 2.2: An example of a REV from the porous media in Figure 2.1.

Two of the notions which are relevant for flow in porous media are saturation and porosity. Saturation describes how much there is of each content in a porous medium, for instance how much water there is in comparison to air in the voids. In this case, the water is called the wetting phase and the air is called the nonwetting phase. Nevertheless, there can be several phases in a flow in porous media, and the sum of the saturations of all the phases is always equal to one in a fully saturated porous medium. The saturation of phase α is defined as (Bear, 1988)

$$s_\alpha = \frac{\text{volume of phase } \alpha}{\text{volume of voids in REV}} \ ,$$

where $s_\alpha \in (0, 1)$ and

$$\sum_\alpha s_\alpha = 1 \ .$$

Porosity on the other hand, describes how porous the medium is. It is defined as the ratio of volume of the void space to the volume of the REV (Bear, 1988)

$$\phi = \frac{\text{volume of voids}}{\text{volume of REV}} \ , \tag{2.1}$$

where $\phi \in (0, 1)$.

2.1 Darcy's law

The Darcy law is one of the most important equations in porous media. It was Henry Darcy who in 1856 introduced the idea and performed the experiments that eventually led to the Darcy law. The most famous experiment Darcy performed was when he packed a column full of sand and then let water flow through it. He made several observations in this experiment, including that the volumetric flow rate q_{Darcy} is proportional to the difference in height, that the flow rate is proportional to the cross-sectional area of the column, and that the flow rate is inversely proportional to the distance between the measurement points, ℓ.

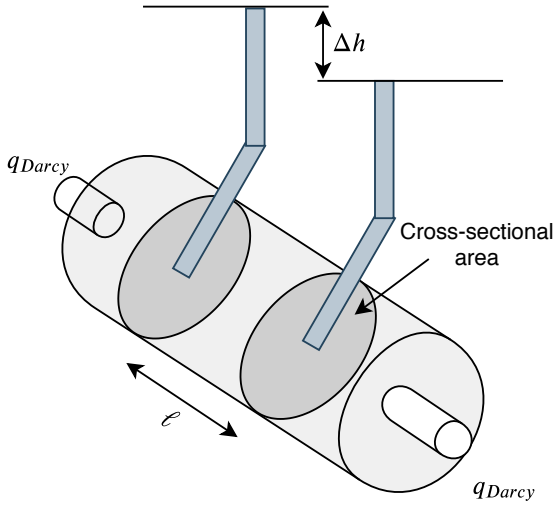

Figure 2.3: Illustration of Darcy's experiment, inspired by (Nordbotten and Celia, 2011).

With his experiments he managed to predict the amount of water that would flow through the sand filters. This law describes the flow in porous media and can be expressed as

$$\boldsymbol{w} = \boldsymbol{\kappa}\frac{h_2 - h_1}{\ell} \ ,$$

where $\boldsymbol{w}$ is the volumetric flux, $\boldsymbol{\kappa}$ is a coefficient of proportionality, h_2 and h_1 are the heights up to which the water in the tubes penetrating the column rises, and ℓ is the length of the column (Nordbotten and Celia, 2011).

The coefficient of proportionality is called the hydraulic conductivity and is given

by

$$\boldsymbol{\kappa} = \frac{\boldsymbol{k}\rho g}{\mu} \ ,$$

where $\boldsymbol{k}$ is the permeability, dependent on the porous medium, ρ is the density of the fluid, g is the gravitational acceleration constant, and μ is the dynamic viscosity of the fluid. This is a function of both porous medium and fluid, and it indicates the ease with which a fluid flows through the material (Nordbotten and Celia, 2011).

The state of a fluid is described by its energy, hence we can derive the hydraulic head from the energy equation defined by $mgh = pV + mgz$. In other words, the potential energy is equal to the pressure potential plus the gravity potential. This will then lead to the hydraulic head being defined as $h = \frac{p}{\rho g} + z$, where z is the height opposite the gravitational direction measured from a reference level we call datum. When saying that the fluid state can be described by its energy, we have made two assumptions:

A1: That the fluid flow is so slow that the kinetic energy can be neglected.
A2: That the fluid is not influenced by temperature or dissolved substances.

Writing the Darcy law in a differential form, it reads

$$\boldsymbol{w} = -\boldsymbol{\kappa}\nabla h \ ,$$

with h being the hydraulic head. In a porous medium, a fluid will flow from regions with higher values of h to regions with lower values of h (Nordbotten and Celia, 2011).

2.2 Mass conservation

When solving for fluid flow in a porous medium, we need to introduce another equation in order to obtain a complete system, as the Darcy law has a number of unknowns that is larger than the number of equations. The equation introduced is the mass conservation equation. The governing idea of this equation is that the change of mass in an arbitrary volume, W, within the domain, Ω, is balanced by the net mass flow into the volume through its boundary and by any mass added to the

volume not associated to the boundary flux. This idea is described by the equation

$$\int_{\Omega} \frac{\partial m}{\partial t} dV = -\int_{\partial\Omega} \boldsymbol{f}\boldsymbol{\nu_m} dA + \int_{\Omega} \Psi dV \ , \tag{2.2}$$

where m is mass per total volume of porous media, $\boldsymbol{f}$ is the mass flux vector, $\boldsymbol{\nu_m}$ is the outward unit vector of $\partial\Omega$ and Ψ is the sink/source within the volume. When Ψ is known external sources or equal to zero, m is a locally conserved quantity for the system and Equation 2.2 is named the mass conservation law (Nordbotten and Celia, 2011).

In the mass conservation law we define $m = \rho\phi = \frac{\text{mass}}{\text{volume of REV}}$ and $\boldsymbol{f} = \rho\boldsymbol{w}$. Using these definitions and the Gauss' theorem, our equation becomes

$$\int_{W} \Big(\frac{\partial \rho\phi}{\partial t} + \nabla \cdot (\rho\boldsymbol{w} - \Psi) \Big) dV = 0 \ ,$$

which holds for arbitrary volumes W. This gives us our final equation for mass conservation of the fluid in differential form as

$$\frac{\partial \rho\phi}{\partial t} + \nabla \cdot (\rho\boldsymbol{w}) = \Psi \ . \tag{2.3}$$

Coupling Equation 2.3 with the Darcy law, we get an equal number of equations and unknowns, hence we now have a complete system and can solve for fluid flow in a porous medium. The final system for single-phase flow reads

$$\boldsymbol{w} = -\frac{\boldsymbol{k}}{\mu}(\nabla p - \rho\boldsymbol{g}) \ , \tag{2.4}$$

$$\frac{\partial \rho\phi}{\partial t} + \nabla \cdot \rho\boldsymbol{w} = \Psi \ , \tag{2.5}$$

where ϕ is the porosity given by Equation 2.1, and Ψ is the source/sink term within the volume (Nordbotten and Celia, 2011).

The Biot model is an extension of the above system to the case of an elastic solid skeleton.

2.3 Transport equation

When the source/sink term within the volume is represented by internal changes of the system, Equation 2.2 is called a transport equation.

In this thesis the transport equation, which models mass transfer in our system, reads

$$\partial_t c - \nabla \cdot \big(D\nabla c - \boldsymbol{w}c\big) = S_c + R(c) \ , \tag{2.6}$$

where c is the concentration, D is the mass diffusivity, and $\boldsymbol{w}$ is the flow field, which in this case is the Darcy flux, i.e. $\boldsymbol{w} = -\boldsymbol{\kappa}\nabla h$. The pure source/sink term, S_c, describes the creation or destruction of substance in the system, and the reaction term, $R(c)$, describes the creation or destruction of the substance as a reaction to itself.

The diffusive term in Equation 2.6 is $\nabla \cdot \big(D\nabla c\big)$. This term describes the movement of substance from an area of high concentration to an area of low concentration.

The advective term in Equation 2.6 is $\nabla \cdot \big(\boldsymbol{w}c\big)$. This describes the movement of substance with the flow field $\boldsymbol{w}$ within the medium.

2.4 Biot equations

In one of his first articles, Maurice A. Biot explains consolidation and how the mechanics of this phenomenon can be applied to an elastic, porous material (Biot, 1941). This theory is important to derive the Biot equations that will be used in our modeling. We will assume, as Biot did, that "the skeleton is purely elastic and contains a compressible viscous fluid" (Biot, 1955).

The Biot equations results in a system of coupled equations that models flow in deformable porous media. The quasi-static system which models a linearly elastic porous medium and is saturated with a slightly compressible fluid can be represented by a momentum conservation equation, and a mass conservation equation, together with the Darcy law. A quasi-static system is a system where the strain rate is very low, meaning that the load is applied so slowly that the structure deforms very

slowly. These equations read

$$-\nabla \cdot \left[2\mu\varepsilon(\boldsymbol{u}) + \lambda\nabla \cdot \boldsymbol{u}\right] + \alpha\nabla p = \boldsymbol{f} \ , \tag{2.7}$$

$$\partial_t\Big(\frac{p}{M} + \alpha\nabla \cdot \boldsymbol{u}\Big) + \nabla \cdot \boldsymbol{w} = S_f \ , \tag{2.8}$$

$$\boldsymbol{K}^{-1}\boldsymbol{w} + \nabla p = \rho_f \boldsymbol{g} \ , \tag{2.9}$$

where μ and λ are the Lamé parameters, $\varepsilon(\boldsymbol{u}) = 0.5(\nabla\boldsymbol{u} + \nabla\boldsymbol{u}^\top)$ is the linearized strain tensor, $\boldsymbol{u}$ is the displacement, α is the Biot-Willis constant which accounts for the pressure-deformation coupling, p is the fluid pressure, $\boldsymbol{f}$ and S_f are source terms, M is the Biot modulus, $\boldsymbol{w}$ is the Darcy flux, $\boldsymbol{K}$ is the permeability tensor divided by fluid viscosity, ρ_f is the fluid density, and $\boldsymbol{g}$ is the gravity vector (Showalter, 2000), (Both et al., 2017).

The equations are fully coupled since they have a physical connection in that fast compression of the medium relative to the fluid flow rate leads to increased pore pressure, and an increase in pore pressure induces a dilation of the medium (Showalter, 2000).

Equation 2.7 represents the linear momentum balance of the system. This is derived from a simple stress formulation, $-\nabla \cdot \boldsymbol{\sigma} = \boldsymbol{f}$ with $\boldsymbol{\sigma} = 2\mu\varepsilon(\boldsymbol{u}) + \lambda\nabla \cdot \boldsymbol{u}\mathbf{I} - \alpha p\mathbf{I}$ being the poroelastic stress (Coussy, 2004). As Equation 2.7 is derived using the St Venant-Kirchhoff-model, we can only allow small deformations in our problem. This is due to the fact that the St Venant-Kirchhoff-model can be unstable for large strains and rotations (Dyke and Hoger, 2000).
The Lamé parameters μ and λ are the shear and dilation moduli of elasticity, respectively. The term $-\alpha p\mathbf{I}$ represents the additional isotropic stress contribution coming from the saturating fluid within the porous material (Showalter, 2000).

Equation 2.8 represents the mass conservation of the fluid. Since we consider only a slightly compressible fluid, we can assume mass conservation is equal to volume conservation, and Equation 2.3 will then read

$$\frac{\partial V}{\partial t} + \nabla \cdot (\rho\boldsymbol{w}) = \Psi \ ,$$

with V being the volume of the fluid. The volume of the fluid is defined as saturation

of the fluid, s_w, times the porosity of the system, ϕ. As we consider a fully saturated flow, $s_w = 1$ and consequently $V = \phi$. The porosity is dependent on the volumetric deformation, $\nabla \cdot \boldsymbol{u}$, and the fluid pressure, p (Dyke and Hoger, 2000). It changes linearly and reads

$$V = \phi(\boldsymbol{u}, p) = \phi_0 + \alpha \nabla \cdot (\boldsymbol{u} - \boldsymbol{u}_0) + \frac{1}{M}(p - p_0) \ ,$$

where ϕ_0 is the initial porosity, $\boldsymbol{u}_0$ is the initial displacement and p_0 is the initial fluid pressure.
The term $\alpha \nabla \cdot \boldsymbol{u}$ represents the additional fluid content due to local volume change. One over the Biot modulus, $\frac{1}{M}$, is a constant combining the compressibility and porosity and describes the amount of fluid which can be forced into the medium (Showalter, 2000).

Equation 2.9 is simply the Darcy law, which is explained in detail in Section 2.1.

Chapter 3

Numerical Scheme

When solving the coupled model with the Biot equations 2.7, 2.8, 2.9 and the transport equation 2.6 numerically, we employ the open-source finite element library FEniCS (Logg et al., 2012). FEniCS is a computing platform for solving partial differential equations, where scientific models are translated to finite element code. In this chapter we will explain some of the mathematics behind this software, starting with time discretization.

3.1 Time discretization

To discretize means to transform a continuum into a discrete, finite subspace. When doing so, the functions defined on the continuum are restricted to the discrete set, allowing restricted functions which are easier to solve. For a time-dependent problem, the domain often observed is the interval $[0, T]$, where T is the final time. If a uniform time discretization is desired, this interval is then partitioned with nodes chosen as $0 = t_0 < t_1 < \ldots < t_n < t_{n+1} = T$, where $t_i = ih$ and $h = \frac{1}{(n+1)}$ (Cheney, 2001).

The basic idea behind numerical methods is to discretize the given continuous problem, with infinitely many degrees of freedom, in order to achieve a discrete problem with a finite number of unknowns. With a finite number of unknowns, the problem is now computational (Johnson, 1987).

There are several numerical methods for approximating the solution of the time-dependent problem given as

$$\begin{cases} y'(t) = f(t, y) \ , \\ y(0) = y_0 \ . \end{cases}$$

The methods usually use an equation, that differs between the methods, to numerically estimate the exact solution, $\{y(t_n)\}_{n=0,1,..}$, of the time-dependent problem. This is done in each node, which in this regard is in each time step. The method is iterated until the sequence of numerically estimated values, $\{y_n\}_{n=1,2,3..}$, converges, or a stopping criterion is reached (Iserles, 2008). A widely used numerical method for the time-dependent problem is the backward Euler method. In this method the next approximated value, y_{n+1}, is found by

$$y_{n+1} = y_n + hf(t_{n+1}, y_{n+1}) \ , \tag{3.1}$$

where, y_{n+1} and y_n is the approximated value of $y(t_n)$ and $y(t_{n+1})$, respectively, h is the time step and $f(t_{n+1}, y_{n+1})$ is the function $y'(t)$ evaluated at the next time step $t = t_{n+1}$.

By rearranging Equation 3.1, we obtain

$$\frac{y_{n+1} - y_n}{h} = f(t_{n+1}, y_{n+1}) \ .$$

This is an implicit method, which means that the new approximation y_{n+1} is present on both sides of the equation. In order to solve the equation for y_{n+1}, an iterative solver or a nonlinear solver should be implemented.

The backward Euler method is a numerically stable method, though computationally expensive since a linear system must be solved at each iteration.

3.2 Finite Element Method

The finite element method is used to approximate the solutions of boundary value problems, which are differential equations together with boundary conditions. These

problems are often used to model physical behavior, for example in association with waves, electrostatics or fluid flow. Many such problems cannot be solved analytically, in which case the finite element method is very useful.

The method goes as follows, where the first step is to reformulate the given differential equation and boundary conditions to a variational formulation,

$$\text{Find } u \in V \quad \text{such that} \quad a(u,v) = \langle \ell, v \rangle \quad \forall v \in V \ , \tag{3.2}$$

where u is the solution of the boundary value problem, v is a test function, V is the Hilbert space which contains the test function v, and $\langle \cdot, \cdot \rangle$ denotes the inner product.

Definition 3.1 (Hilbert space). *A Hilbert space is a complete, normed vector space V with $\|x\| = \sqrt{\langle x, x \rangle}$ $\forall x \in V$.* ⌟

Furthermore, $a : V \times V \to \mathbb{R}$ is a symmetric positive bilinear form and $\ell : V \to \mathbb{R}$ is a linear functional (Braess, 2007).
The variational formulation is achieved by multiplying the differential equation in the boundary value problem with the test function v, and then integrating over the domain the equation lies in.
For example, if the differential equation is given as the Poisson equation

$$\begin{cases} -\nabla \cdot \nabla u = f & \text{in } \Omega \ , \\ u = 0 & \text{on } \partial\Omega \ , \end{cases}$$

where Ω is a connected bounded domain in $\mathbb{R}^n$, $\partial\Omega$ is the boundary of Ω and f is a continuous function on Ω. Then by multiplying u with v and integrating over Ω, the variational formulation 3.2 becomes

$$\text{Find } u \in V \quad \text{such that} \quad \int_\Omega \nabla u \cdot \nabla v dx = \int_\Omega f v dx \quad \forall v \in V \ .$$

The boundary conditions are divided into *essential* and *natural* boundary conditions, where the essential ones are explicitly built into the function space, while the natural ones has to be implicitly forced (Braess, 2007). These boundary conditions are called

Dirichlet and Neumann boundary conditions, respectively.

The next step in the finite element method is to construct a mesh of the given domain. This is done by partitioning the domain into elements, which for the two-dimensional case can be either triangles or quadrilaterals, and consider functions which reduce to a polynomial in each element (Braess, 2007). The vertices of the elements are defined to be the nodes of the domain.

An approximation space $V_h \subset V$ can then be constructed. The approximation space is spanned by a set of basis functions φ_i and is finite dimensional. This approach of discretization in the finite element method is called the *Galerkin method* (Knabner and Angermann, 2003). In a discrete form, 3.2 now reads,

$$\text{Find } u_h \in V_h \quad \text{such that} \quad a(u_h, v_h) = \langle \ell, v_h \rangle \quad \forall v_h \in V_h \ . \tag{3.3}$$

Since V_h is a finite dimensional space, it is now possible to find the solution explicitly.

Furthermore, we find the approximated linear system by first defining the approximated solution u_h as the sum of all basis functions multiplied by η_i, where the η_i's are the coefficients in the expansion of u_h in the basis functions φ_i, and N is the dimension of V_h,

$$u_h = \sum_{i=1}^{N} \eta_i \varphi_i \ .$$

We then substitute the approximated solution into 3.3, test with $v_h = \varphi_j$, and rewrite it as a linear system,

$$\sum_{i=1}^{N} a_{ij} \eta_i = b_j \quad \forall j = 1 : N \ ,$$

where $a_{ij} = a(\varphi_i, \varphi_j)$ and $b_j = \langle \ell, \varphi_j \rangle$. This is now a complete system with N equations and N unknowns. By solving this linear system for the η_i's, we will approximate the solution of the given boundary value problem.

We then study the error to see if our approximation is accurate enough. How the error is studied in this thesis is discussed in Section 4.2.

3.3 Iterative schemes

Iterative schemes are used to find the approximated solution of a problem. Iteration refers to a repetitive process, which is the principle behind these schemes. In the first step, an initial guess for the solution has to be made in order to initiate the iterative process. This initial guess is then used to compute a sequence of approximate solutions of increasing accuracy. The algorithm for a fixed-point iterative scheme reads,

$$\text{For } x_0 \text{ given}, \quad \text{let } x_{n+1} = Fx_n, \quad n = 0, 1, 2, \dots ,$$

where x_0 is the initial guess, x_n is the approximated solution from the previous step and x_{n+1} is the approximated solution for this step (Cheney, 2001). This is repeated until the approximated solution is sufficiently close to the real solution.

There are several ways to perform iteration on a set of equations. In the coupling of flow and mechanics in porous media, one approach which is commonly used, and extensively researched, is a splitting-based iterative method. In this method the two systems are split into two sub-problems which can be solved directly. If the sub-problem for the mechanics is solved first, the method is referred to as the *undrained split* or *drained split* iterative method, while if the sub-problem for the flow is solved first, the method is referred to as the *fixed stress split* or *fixed strain split* iterative method.

In the drained split method, the pressure field is frozen when solving the mechanics sub-problem, meaning there is no change in pressure. When the sub-problem for the flow is solved, the displacement field is frozen.

In the fixed strain split method, the strain field is frozen when the flow sub-problem is solved. Following this, the sub-problem for the mechanics is solved exactly.

These two methods are conditionally stable, depending on the strength of the coupling between the two sub-problems. This can cause oscillations in the numerical solutions obtained, making them an unattractive choice for our problem (Kim et al., 2009).

In the undrained split method, the fluid mass in each gridblock remains constant, while the pressure is allowed to change locally when solving the mechanics sub-

problem.

In the fixed stress split method, the total mean stress field is frozen when solving the flow sub-problem. To keep the rate of mean stress constant, a stabilization parameter defined by $L = \frac{\alpha^2}{K_{dr}}$ is introduced. It has been analyzed in literature that in the case of convergence, the stabilization terms vanish, hence introducing this parameter does not alter the equation for convergent systems. The sub-problem for the mechanics is then solved exactly.

These two methods are unconditionally stable, and do not depend on the coupling between the sub-problems. In the research done by Kim et al. (2009), the fixed stress split method is proven to converge faster than the undrained split method when performing a von Neumann stability analysis. This is proved extensively and for more generalized cases in (Mikelić and Wheeler, 2013). In (Mikelić and Wheeler, 2013) they also prove that choosing $L = \frac{\alpha^2}{2K_{dr}}$ causes the fixed stress split iterative method to converge even faster. This, in addition to having no oscillations in the numerical solutions, makes the fixed stress split iterative method the best choice for the problem studied in this thesis. The fixed stress split method is used on the Biot equations in (Bause et al., 2017), (Both et al., 2017), (Borregales et al., 2018), (Both et al., 2019), (Storvik et al., 2018), (Brun et al., 2019), (Borregales et al., 2019) where it has proven to be a stable, robust method. In (Bause et al., 2017) and (Storvik et al., 2018) they focused on optimizing L by two different approaches, in (Both et al., 2017) a heterogeneous porous media is considered, while in (Borregales et al., 2018) non-linearities in the fluid flow and mechanical deformation are studied. Both et al. (2019) studied an unsaturated media where the Biot model is coupled with the Richardson equation, and an Anderson acceleration is applied, and Brun et al. (2019) studied a thermo-poroelastic five-field model. Finally, in (Borregales et al., 2019) a parallel-in-time fixed stress splitting scheme is studied.

3.4 Extension to the Biot Equations and Transport Equation

Before extending these numerical schemes to the Biot equations, 2.7, 2.8, 2.9, and the transport equation, 2.6, we need to make a few assumptions on the mathematical model and data:

A1: $\mu, \lambda, \alpha, M, D$ are all positive.

A2: The fluid viscosity is constant.

A3: $\boldsymbol{K}$ is symmetric, bounded and constant in time.

A4: We are considering a two-dimensional problem, hence $\boldsymbol{g}$ is zero.

A5: $\boldsymbol{u} = \boldsymbol{0}, p = 0, c = 0$ on the boundary, for simplicity.

A6: $\boldsymbol{u} = \boldsymbol{u}_0$, $p = p_0$, $c = c_0$ are initial conditions.

We will now apply the finite element method from Section 3.2 on the Biot equations, 2.7, 2.8, 2.9. A mixed formulation is applied for the flow in order to define flux as a separate unknown and thereby obtain a system of first-order equations for the flow. This approach is commonly used, as it is locally mass conservative and the computation of the flux is explicit (Almani et al., 2016).

Consider a space-time domain $\Omega \times (0, T)$ with $\Omega \subset \mathbb{R}^2$. Partition Ω into triangular elements with linear Galerkin elements for the displacement, discontinuous Galerkin elements for the pressure and lowest order Raviart-Thomas elements for the flux. These elements are chosen in such a way that the system of equations become sparse and consequently unexpensive to solve computationally. The time interval $(0, T)$ is discretized with nodes chosen as $0 = t_0 < t_1 < \ldots < t_n < t_{n+1} = T$, $n \in \mathbb{N}$, and step size chosen as $\Delta t = \frac{1}{(n+1)}$, as previously demonstrated in Section 3.1.

With these space discretizations, we can now define the approximation spaces for the Biot equations. Let $\mathcal{T}_h$ be a regular triangulation of Ω with mesh size h, $\mathcal{E}_\Omega$ be the set of all interior edges, and $\mathcal{P}_0, \mathcal{P}_1$ be the spaces of constant and linear polynomials

respectively. Then the approximation spaces are given by

$$\boldsymbol{V}_h = \left\{ \boldsymbol{v}_h \in [H_0^1(\Omega)]^2 \mid \forall T \in \mathcal{T}_h,\ \boldsymbol{v}_h|_T \in [\mathcal{P}_1]^2 \right\}, \tag{3.4}$$

$$Q_h = \left\{ q_h \in L^2(\Omega) \mid \forall T \in \mathcal{T}_h,\ q_h|_T \in \mathcal{P}_0 \right\}, \tag{3.5}$$

$$\boldsymbol{Z}_h = \left\{ \boldsymbol{z}_h \in H(\mathrm{div};\Omega) \mid \forall T \in \mathcal{T}_h\ \exists \boldsymbol{a} \in \mathbb{R}^2\ \exists b \in \mathbb{R}\ \forall x \in T,\ \boldsymbol{z}_h(\boldsymbol{x}) = \boldsymbol{a} + b\boldsymbol{x} \right.$$
$$\left. \text{and } \forall E \in \mathcal{E}_\Omega, [z]_E \cdot \nu_E = 0 \right\}, \tag{3.6}$$

where $L^2(\Omega)$ is the Hilbert space of square integrable functions, $H_0^1(\Omega)$ is the Hilbert space of square integrable functions which vanishes on the domain boundary, admitting weak derivatives of first order in the same space, and $H(\mathrm{div};\Omega)$ is the Hilbert space of vector-valued square integrable functions admitting a weak divergence in the same space. The same discretization was used in e.g. (Both et al., 2017). For more details on the discretization of H(div) see e.g. (Bahriawati and Carstensen, 2005).

As there is a time derivative present in Equation 2.8, this term should be discretized in time. Since we plan on using an iterative approach, an implicit method is clearly the most appropriate choice for the time discretization. We will use a backward Euler method, which was presented in Section 3.1. The reason for choosing this particular discretization is the stability it provides for large time steps. The Biot equations models an infinitesimally deforming porous media, hence it is important to observe the model for a longer period of time. In this thesis we will observe the model for 10 seconds.
The backward Euler method replaces $\partial_t p$ in Equation 2.8 with $\frac{p^{n+1}-p^n}{\Delta t}$, and we can now solve the complete system of Biot equations without a time derivative present.

Remark 1 (Notation). In the following, two indices will at times be present. To clarify, the one denoted by n is the time step, and the other, which is denoted by i, is the iteration index.

Let the initial conditions $(\boldsymbol{u}_h^0, p_h^0, \boldsymbol{w}_h^0) \in \boldsymbol{V}_h \times Q_h \times \boldsymbol{Z}_h$ be given. The discrete

variational formulation, as seen in e.g. (Both et al., 2017), for the Biot equations then reads:
Given $(\boldsymbol{u}_h^{n-1}, p_h^{n-1}, \boldsymbol{w}_h^{n-1}) \in \boldsymbol{V}_h \times Q_h \times \boldsymbol{Z}_h$ for all $n \in \mathbb{N}, n \geq 1$, find $(\boldsymbol{u}_h^n, p_h^n, \boldsymbol{w}_h^n) \in \boldsymbol{V}_h \times Q_h \times \boldsymbol{Z}_h$ such that for all $(\boldsymbol{v}_h, q_h, \boldsymbol{z}_h) \in \boldsymbol{V}_h \times Q_h \times \boldsymbol{Z}_h$

$$\langle 2\mu\varepsilon(\boldsymbol{u}_h^n), \varepsilon(\boldsymbol{v}_h)\rangle + \langle \lambda\nabla\cdot\boldsymbol{u}_h^n, \nabla\cdot\ \boldsymbol{v}_h\rangle - \langle \alpha p_h^n, \nabla\cdot\boldsymbol{v}_h\rangle = \langle \boldsymbol{f}, \boldsymbol{v}_h\rangle\ , \tag{3.7}$$

$$\left\langle \frac{1}{M} p_h^n, q_h \right\rangle + \langle \alpha\nabla\cdot\boldsymbol{u}_h^n, q_h\rangle + \Delta t\langle \nabla\cdot\boldsymbol{w}_h^n, q_h\rangle =$$

$$\Delta t\langle S_f, q_h\rangle + \left\langle \frac{1}{M} p_h^{n-1}, q_h \right\rangle + \langle \alpha\nabla\cdot\boldsymbol{u}_h^{n-1}, q_h\rangle\ , \tag{3.8}$$

$$\langle \boldsymbol{K}^{-1}\boldsymbol{w}_h^n, \boldsymbol{z}_h\rangle - \langle p_h^n, \nabla\cdot\boldsymbol{z}_h\rangle = 0\ . \tag{3.9}$$

This system of equations can now be solved as a fully coupled system, or the flow and mechanics can be decoupled and solved in an iterative way, as presented in Section 3.3. We will choose the latter approach for this thesis, as the fixed stress split iterative method has shown to be a good choice for our problem.

Furthermore, we also need to discretize the transport equation, 2.6, in space and time to be able to solve the Biot equations and the transport equation simultaneously. To discretize in space, we follow the finite element method from Section 3.2.

Consider the same space-time domain as for the Biot equations. Partition now Ω into triangular elements with linear Galerkin elements. The time interval is partitioned such as for the Biot equations. With these discretizations, the approximation space for the transport equation is given by

$$B_h = \left\{ b_h \in H^1(\Omega) \mid \forall T \in \mathcal{T}_h,\ b_h|_T \in \mathcal{P}_1 \right\}\ . \tag{3.10}$$

Since there is a time derivative present in Equation 2.6 as well, the backward Euler method is applied here too. $\partial_t c$ is replaced with $\frac{c^{n+1}-c^n}{\Delta t}$, removing the time derivative in this equation as well.

Let the initial condition $c_h^0 \in B_h$ be given. The discrete variational formulation for the transport equation then reads:

Given $c_h^{n-1} \in B_h$ for all $n \in \mathbb{N}, n \geq 1$, find $c_h^n \in B_h$ such that for all $b_h \in B_h$

$$\langle c_h^n, b_h\rangle + \Delta t\langle D\nabla c_h^n, \nabla b_h\rangle + \Delta t\langle \nabla c_h^n \cdot \boldsymbol{w}_h^n, b_h\rangle + \Delta t\langle c_h^n \nabla \cdot \boldsymbol{w}_h^n, b_h\rangle = \Delta t\langle S_c, b_h\rangle + \Delta t\langle R(c_h^n), b_h\rangle + \langle c_h^{n-1}, b_h\rangle \ . \tag{3.11}$$

We will now use the fixed stress split iterative method to approximate the Biot equations 3.7, 3.8, 3.9 and the transport equation 3.11. For linearization of the reaction term in Equation 3.11, the L-scheme is employed as a linearization technique as well as stabilization, such as in e.g. (List and Radu, 2016), (Borregales et al., 2018), (Brun et al., 2019).

By initializing $\boldsymbol{u}_h^{n,0} = \boldsymbol{u}_h^{n-1}$, $p_h^{n,0} = p_h^{n-1}$, $\boldsymbol{w}_h^{n,0} = \boldsymbol{w}_h^{n-1}$, and $c_h^{n,0} = c_h^{n-1}$, the fixed stress split iterative method gives us a sequence of approximations $(\boldsymbol{u}_h^{n,i}, p_h^{n,i}, \boldsymbol{w}_h^{n,i}, c_h^{n,i})$, $i \geq 0$. The flow sub-problem is solved first while the total mean stress field is frozen, meaning that $\sigma_\beta = \sigma_0 + K_{dr}\nabla \cdot \boldsymbol{u} - \alpha p$ is kept constant by introducing the tuning parameter L (Both et al., 2017). Next, the mechanics sub-problem is solved using the approximated solution for pressure from the flow sub-problem. After this, the transport equation is solved using the approximated solution for the flux. This iteration process is continued until a specified tolerance is reached.

The iterative procedure consists of three steps which reads as follows:
Step 1: For $i \geq 1$, find $(p_h^{n,i}, \boldsymbol{w}_h^{n,i}) \in Q_h \times \boldsymbol{Z}_h$ given $(\boldsymbol{u}_h^{n,i-1}, p_h^{n,i-1}, \boldsymbol{w}_h^{n,i-1}) \in \boldsymbol{V}_h \times Q_h \times \boldsymbol{Z}_h$ such that for all $(q_h, \boldsymbol{z}_h) \in Q_h \times \boldsymbol{Z}_h$ there holds

$$\left\langle \left(\frac{1}{M} + L_1\right) p_h^{n,i}, q_h \right\rangle + \Delta t\ \langle \nabla \cdot \boldsymbol{w}_h^{n,i}, q_h\rangle = \Delta t\langle S_f, q_h\rangle + \left\langle \frac{1}{M} p_h^{n-1}, q_h \right\rangle + \langle \alpha \nabla \cdot \boldsymbol{u}_h^{n-1}, q_h\rangle + \langle L_1 p_h^{n,i-1}, q_h\rangle - \langle \alpha \nabla \cdot \boldsymbol{u}_h^{n,i-1}, q_h\rangle \ , \tag{3.12}$$

$$\langle \boldsymbol{K}^{-1}\boldsymbol{w}_h^{n,i}, \boldsymbol{z}_h\rangle - \langle p_h^{n,i}, \nabla \cdot \boldsymbol{z}_h\rangle = 0 \ . \tag{3.13}$$

Step 2: Find $\boldsymbol{u}_h^{n,i} \in \boldsymbol{V}_h$ given $p_h^{n,i} \in Q_h$ such that for all $\boldsymbol{v}_h \in \boldsymbol{V}_h$ there holds

$$\langle 2\mu\varepsilon(\boldsymbol{u}_h^{n,i}), \varepsilon(\boldsymbol{v}_h)\rangle + \langle \lambda \nabla \cdot \boldsymbol{u}_h^{n,i}, \nabla \cdot \boldsymbol{v}_h\rangle = \langle \boldsymbol{f}, \boldsymbol{v}_h\rangle + \langle \alpha p_h^{n,i}, \nabla \cdot \boldsymbol{v}_h\rangle \ . \tag{3.14}$$

Step 3: Find $c_h^{n,i} \in B_h$ given $\boldsymbol{w}_h^{n,i} \in \boldsymbol{Z}_h$, $c_h^{n,i-1} \in B_h$ such that for all $b_h \in B_h$ there holds

$$\langle c_h^{n,i}, b_h\rangle + \Delta t\langle D\nabla c_h^{n,i}, \nabla b_h\rangle + \Delta t\langle \nabla c_h^{n,i} \cdot \boldsymbol{w}_h^{n,i}, b_h\rangle + \Delta t\langle c_h^{n,i}\nabla \cdot \boldsymbol{w}_h^{n,i}, b_h\rangle + \langle L_2 c_h^{n,i}, b_h\rangle = \Delta t\langle S_c, b_h\rangle + \Delta t\langle R(c_h^{n,i-1}), b_h\rangle + \langle c_h^{n-1}, b_h\rangle + \langle L_2 c_h^{n,i-1}, b_h\rangle \ . \tag{3.15}$$

Remark 2. We want to call attention to the different L's, and specify these two. L_1 is the stabilization term introduced by the the fixed stress splitting scheme, as discussed in Section 3.3, and L_2 is the stabilization term introduced to linearize the reaction term and to stabilize the iterative scheme, given as a positive constant. L_2 should be chosen as small as possible in order to increase convergence rate, but also large enough to ensure a stabilizing effect (List and Radu, 2016).

We now have an algorithm on how to solve the decoupled Biot equations coupled with the nonlinear transport equation.

Chapter 4

Numerical Results

In this chapter we will analyze the robustness of the fixed stress split iterative method when coupling the Biot equations 2.7, 2.8, 2.9, with the the transport equation 2.6. Furthermore, we will study the efficiency of this iterative method compared to the monolithic approach.
We will consider three different test cases for the reaction term in the transport equation;

1. $R(c) = 0$.
2. $R(c) = Ac$.
3. $R(c) = \frac{Ac}{A+c}$.
4. $R(c) = c^2$.

On two domains;

1. The unit square.
2. The L-shaped domain.

4.1 Code validation

For the implementation of this scheme, we use FEniCS software (Langtangen and Logg, 2017). The stopping criterion employed is $\|(\boldsymbol{u}^i, p^i, \boldsymbol{w}^i, c^i) - (\boldsymbol{u}^{i-1}, p^{i-1}, \boldsymbol{w}^{i-1}, c^{i-1})\| \leq \delta_a + \delta_r \|(\boldsymbol{u}^i, p^i, \boldsymbol{w}^i, c^i)\|$, $\delta_a, \delta_r > 0$, where δ_a, δ_r are the absolute and relative toler-

ances, respectively. In other words, this is saying that the error for the displacement, pressure, flux and concentration at each iteration, should be smaller than an absolute tolerance plus a relative tolerance multiplied with the associated norm. The physical parameters used in our numerical analysis are the same as the ones used in (Mikelić et al., 2014) for the Mandel's problem, a benchmark problem for validating coupled flow in elastic porous media. These parameters, and a few others we use in our model, are given in Table 4.1.

Symbol	Quantity	Value
μ	First Lamé parameter	2.475×10^{9}
λ	Second Lamé parameter	1.650×10^{9}
α	Biot-Willis constant	1.0
M	Biot modulus	1.650×10^{10}
D	Mass diffusivity	0.465
A	Reaction coefficient	0.5
$\boldsymbol{K}$	Permeability tensor divided by fluid viscosity	1.0×10^{-14}
d	Dimension	2
ξ	Pressurescale	1.0×10^{12}
δ_a	Absolute tolerance	1.0×10^{-8}
δ_r	Relative tolerance	1.0×10^{-8}
T	Final time	10.0
Δt	Time step size	1.0
h	Space step size for the unit square	0.25, 0.125, 0.0625, 0.03125
h_{min}	Smallest space step size for the L-shape	0.06132, 0.03066, 0.01533, 0.00767

Table 4.1: Input parameters for our problem.

We will test the scheme with three different tuning parameters, introduced by the fixed stress splitting method, to find the optimal choice for our model. The tuning parameters we will evaluate are;

1. $L = \frac{\alpha^2}{\frac{2\mu}{d}+\lambda}$.
2. $L = \frac{\alpha^2}{2\left(\frac{2\mu}{d}+\lambda\right)}$.
3. $L = \frac{\alpha^2}{2\lambda}$.

We will also test the scheme with and without the stabilization terms introduced by linearization of the reaction term in the transport equation. The stabilization parameters, denoted as L_2 in our scheme, evaluated are;

1. $L_2 = 0$.
2. $L_2 = 1.0 \times 10^2$.
3. $L_2 = 1.0 \times 10^{-2}$.
4. $L_2 = 1.0 \times 10^6$.
5. $L_2 = 1.0 \times 10^{-6}$.

To construct a test problem for this scheme, we use the method of manufactured solutions. We observe that the size of the physical values differs greatly, so we add a pressurescale parameter, ξ, to our exact solution of the pressure in order to scale the equations.

4.1.1 The unit square

If we choose our domain to be $\Omega = (0,1) \times (0,1) \subset \mathbb{R}^2$, the exact solutions for the displacement, pressure, flux and concentration reads,

$$\boldsymbol{u}(x,y,t) = \begin{bmatrix} txy(x-1)(y-1) \\ txy(x-1)(y-1) \end{bmatrix} , \tag{4.1}$$

$$p(x,y,t) = \xi txy(x-1)(y-1) , \tag{4.2}$$

$$\boldsymbol{w}(x,y,t) = -\boldsymbol{K}\ \nabla p = \begin{bmatrix} K\xi t(y^2 - 2xy^2 + 2xy - y) \\ K\xi t(x^2 - 2x^2y + 2xy - x) \end{bmatrix} , \tag{4.3}$$

$$c(x,y,t) = txy(x-1)(y-1) . \tag{4.4}$$

Plugging these into the equations, 2.7, 2.8, 2.9, 2.6, we obtain the source terms;

$$\boldsymbol{f} = \begin{bmatrix} \alpha\xi yt(y-1)(2x-1) - 4\mu ty(y-1) - \mu t[(2x-1)(2y-1) + 2x(x-1)] \\ \alpha\xi xt(x-1)(2y-1) - 4\mu tx(x-1) - \mu t[(2x-1)(2y-1) + 2y(y-1)] \\ \qquad\qquad - \lambda t[(2x-1)(2y-1) + 2y(y-1)] \\ \qquad\qquad - \lambda t[(2x-1)(2y-1) + 2x(x-1)] \end{bmatrix},$$

$$\begin{aligned} S_f = \frac{1}{M}\xi(xy(x-1)(y-1)) &+ 2\xi \boldsymbol{K} t(x(x-1) + y(y-1)) \\ &+ \alpha((2x-1)(y-1)y + (2y-1)(x-1)x) \ , \end{aligned}$$

$$\begin{aligned} S_c = Dt(-2x^2 + 2x) + Dt(-2y^2 + 2y) - R(c) - \xi \boldsymbol{K} t^2(x - 2xy + 2x^2y - x^2)^2 \\ -\xi \boldsymbol{K} t^2(y - 2xy + 2xy^2 - y^2)^2 + xy(x-1)(y-1) \\ +\xi \boldsymbol{K} t^2(-2x^2 + 2x)(x^2y^2 - x^2y - xy^2 + xy) \\ +\xi \boldsymbol{K} t^2(-2y^2 + 2y)(x^2y^2 - x^2y - xy^2 + xy) \ . \end{aligned}$$

We solve the equations 3.12, 3.13, 3.14, 3.15, with these source functions on the right-hand side and the exact solutions for the displacement, pressure and concentration as Dirichlet boundary conditions. Since we are using a mixed-formulation for the flow, the Dirichlet boundary condition for the pressure is applied as a natural boundary condition in Equation 3.12 and Equation 3.13.

Following this, we refine the mesh four times in order to analyze the mesh dependency and convergence of the method. Here, we show an example of the coarsest and finest mesh tested. We use the same meshes for the pressure, flux, displacement and concentration.

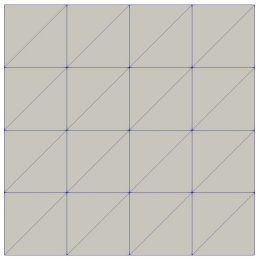

(a) 4x4 mesh

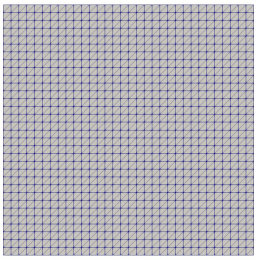

(b) 32x32 mesh

The refinement is caused by taking h to be smaller which again leads to smaller triangles. When the triangles are smaller, the approximated solution is computed in several areas, which gives a solution that is closer to the exact solution.

The approximated solutions we obtain for the finest mesh at the final time $T = 10s$ are given in the following plots;

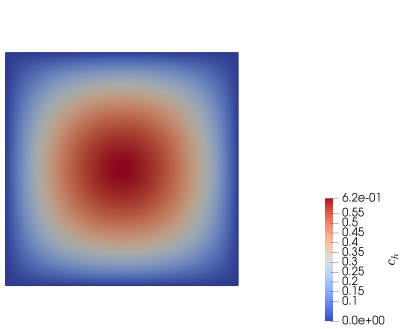

(a) Concentration, c_h

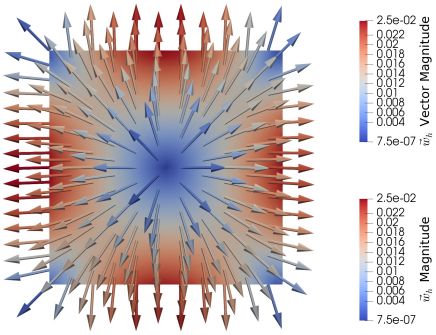

(b) Flux $\boldsymbol{w}_h$ and magnitude

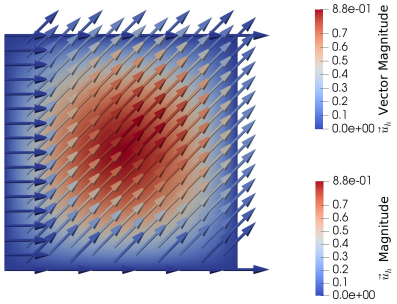

(c) Displacement $\boldsymbol{u}_h$ and magnitude

Figure 4.2: Approximated solutions for concentration, flux and displacement at $T = 10s$.

Remark 3 (Plots). As the concentration, pressure and the two components of the displacement have the same exact solutions, we only show the plot for the concentration. The other plots look exactly the same, only with different values. For the displacement we also show a plot of its magnitude.

By examining the plots and comparing them to the exact solutions, we understand that our scheme approximate the solutions properly.

We now observe the iteration count for different time steps in relation to different tuning parameters L.

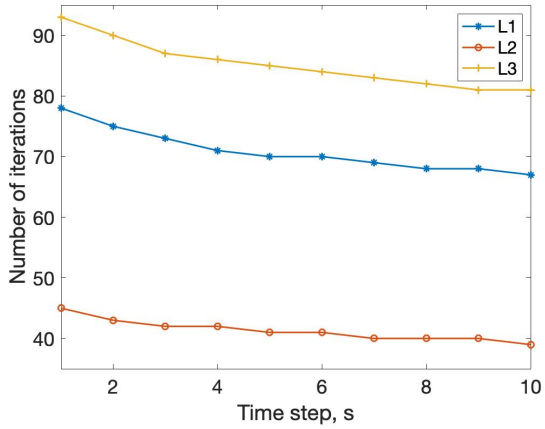

Figure 4.3: L1 = $\frac{\alpha^2}{\frac{2\mu}{d}+\lambda}$, L2 = $\frac{\alpha^2}{2\left(\frac{2\mu}{d}+\lambda\right)}$, L3 = $\frac{\alpha^2}{2\lambda}$.

Clearly, L2 = $\frac{\alpha^2}{2\left(\frac{2\mu}{d}+\lambda\right)}$ gives the best result with the fewest amount of iterations. This is the same result as was shown in (Mikelić and Wheeler, 2013) and (Both et al., 2017), where $L = \frac{\alpha^2}{2(\frac{2\mu}{d}+\lambda)}$ was indeed the optimal choice for L.
Also, the number of iterations should be the same for each mesh size, which is indeed the case in these results.

When we want to test the number of iterations needed to solve only the transport equation, we use the Darcy flux computed at the final iteration of the Biot equations as the flow field in the transport equation, and then iterate the transport equation separately. Testing with different stabilization parameters, L_2, for the transport equation, did not alter the number of iterations in any case. Consequently, we can conclude that our scheme is not sensitive to the stabilization of the transport equation. Additionally, different reaction terms did not change the results, and we draw the conclusion that our method is stable for different choices of $R(c)$. In Table 4.2 we plot the number of iterations needed to solve the transport equation for different reaction terms and stabilization parameters. The number of iterations is the same for every mesh size and is not affected by an implicit or explicit reaction term. When $R(c) = 0$, the number of iterations is the same as when there is a reaction term present.

	$R(c) = Ac$	$R(c) = \frac{Ac}{A+c}$	$R(c) = c^2$
$L_2 = 0$	3	3	3
$L_2 = 1.0 \times 10^2$	3	3	3
$L_2 = 1.0 \times 10^{-2}$	3	3	3
$L_2 = 1.0 \times 10^6$	3	3	3
$L_2 = 1.0 \times 10^{-6}$	3	3	3

Table 4.2: Number of iterations for the transport equation for different reaction terms and stabilization constants.

4.1.2 The L-shaped domain

For the L-shaped domain, which we define as $\Omega = (0,1) \times (0,1) \backslash (0.5,1) \times (0.5,1) \subset \mathbb{R}^2$, we use the same exact solutions and source functions, and we solve the same equations, as for the unit square. The boundary conditions are the same as for the unit square on the boundaries $\Gamma_1 = \{0\} \times (0,1),\ \Gamma_2 = (0,1) \times \{0\},\ \Gamma_3 = (0,0.5) \times \{1\},\ \Gamma_4 = \{1\}\ \times (0,0.5)$. For the boundaries $\Gamma_5 = \{0.5\} \times (0.5,1),\ \Gamma_6 = (0.5,1) \times \{0.5\}$, we apply Neumann boundary conditions for the pressure, displacement and concentration. The Neumann boundary conditions are obtained by multiplying the derivative of the exact solutions with the normal vector of the associated boundary. They appear on the right hand side of the equations, where they are multiplied with the associated test functions and integrated over the belonging boundary. The Neumann boundary condition for the pressure is applied as an essential boundary condition in this case, since we are using a mixed formulation for the flow.

We perform a mesh refinement four times for this mesh as well. The plots show the coarsest and finest mesh tested for the L-shaped domain. We use the same meshes for the pressure, flux, displacement and concentration.

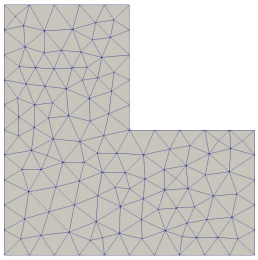

(a) Coarse mesh, $h_{min} = 0.06132$.

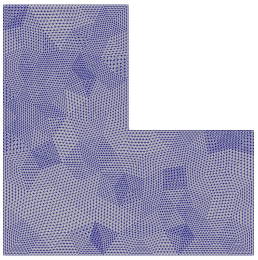

(b) Fine mesh, $h_{min} = 0.00767$.

The approximated solutions we obtain for the finest mesh in this domain are given in the following plots. We will plot the same time step and types of plots as for the unit square.

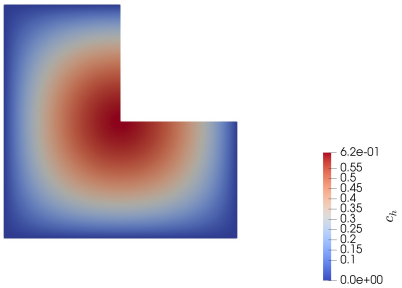

(a) Concentration, c_h

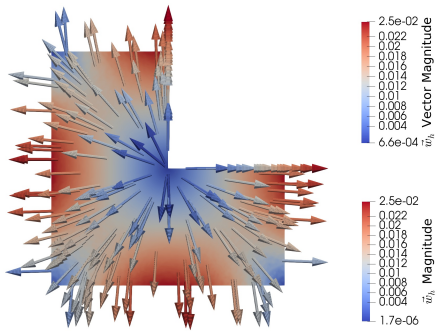

(b) Flux $\boldsymbol{w}_h$ and magnitude

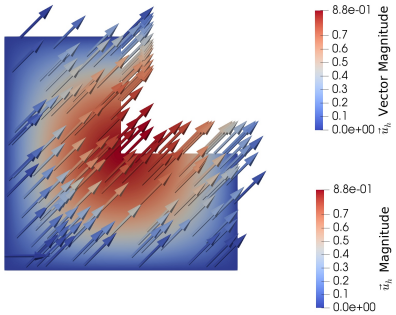

(c) Displacement $\boldsymbol{u}_h$ and magnitude

Figure 4.5: Approximated solutions for concentration, flux and displacement at $T = 10s$.

As a result of choosing Neumann boundary conditions on Γ_5, Γ_6, we observe that

the plots in the L-shaped domain are exactly the same as the plots in the unit square, except that they are missing the top right square. If we had chosen homogeneous Dirichlet boundary conditions on the whole boundary, the plots of concentration, pressure and displacement would be zero on the whole boundary and the exact solutions defined in equations 4.1, 4.2, 4.3, 4.4 would no longer be valid.

We now observe the iteration count for different time steps in relation to different tuning parameters L.

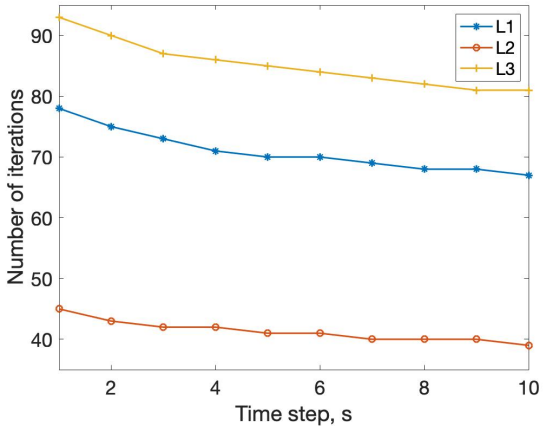

Figure 4.6: L1 = $\frac{\alpha^2}{\frac{2\mu}{d}+\lambda}$, L2 = $\frac{\alpha^2}{2\left(\frac{2\mu}{d}+\lambda\right)}$, L3 = $\frac{\alpha^2}{2\lambda}$.

We observe that the tuning parameter that gives the lowest amount of iterations is L2 = $\frac{\alpha^2}{2\left(\frac{2\mu}{d}+\lambda\right)}$, which is expected. The number of iterations is the same for the different mesh sizes, and for the different reaction terms. These results are the same as for the unit square, and follows the articles published by (Mikelić and Wheeler, 2013), (Both et al., 2017).

When testing the number of iterations needed to solve the transport equation in the L-shaped domain, we use the same approach as for the unit square. The number of iterations is the same for all cases tested in this domain as well. We refer to Table 4.2 for the results. A change in mesh size, or choosing an explicit or implicit reaction term, does not influence the number of iterations in this domain either.

4.1.3 Analysis

Following this, we compare the numerical solutions with the exact analytical solutions to observe the errors. An analyzation of the asymptotic behavior of the error at different space step sizes h can tell us if the program works.

Another test to see if our program works is the iteration count. It was demonstrated in (Both et al., 2017) that the convergence was not influenced by a change in the mesh, hence the iteration count should be the same when we refine the mesh. It is shown in Table 4.3 that this is indeed the case for our simulation. We plot the iteration count for $L = \frac{\alpha^2}{2(\frac{2\mu}{d}+\lambda)}$.

	Unit square				L-shape			
h	0.25	0.125	0.0625	0.03125	0.06132	0.03066	0.01533	0.00767
i	39	39	39	39	39	39	39	39

Table 4.3: Here h is the space step size and i is the number of iterations at the final time step.

4.1.4 Monolithic scheme

We will now study the efficiency of the fixed stress split iterative method by comparing the elapsed time after solving the system iteratively, with the elapsed time after solving the system monolithically. Two different monolithic schemes are considered.

Case 1

In this case, only the Biot equations are solved monolithically, while the transport equation is solved iteratively. The Darcy flux approximated in the fully coupled Biot equations will be used as the flow field in the transport equation. We will use the same stopping criterion for the concentration here, as we did in the fixed stress splitting method.

This procedure consists of two steps which reads as follows:
Step 1: Find $(p_h^n, \boldsymbol{w}_h^n, \boldsymbol{u}_h^n) \in Q_h \times \boldsymbol{Z}_h \times \boldsymbol{V}_h$ given $(p_h^{n-1}, \boldsymbol{w}_h^{n-1}, \boldsymbol{u}_h^{n-1}) \in Q_h \times \boldsymbol{Z}_h \times \boldsymbol{V}_h$

such that for all $(q_h, \boldsymbol{z}_h, \boldsymbol{v}_h) \in Q_h \times \boldsymbol{Z}_h \times \boldsymbol{V}_h$ there holds

$$\begin{aligned}\langle \boldsymbol{K}^{-1}\boldsymbol{w}_h^n, \boldsymbol{z}_h\rangle - \langle p_h^n, \nabla\cdot\boldsymbol{z}_h\rangle + \left\langle \frac{1}{M}p_h^n, q_h\right\rangle + \Delta t\ \langle \nabla\cdot\boldsymbol{w}_h^n, q_h\rangle + \langle 2\mu\varepsilon(\boldsymbol{u}_h^n), \varepsilon(\boldsymbol{v}_h)\rangle \\ + \langle \lambda\nabla\cdot\boldsymbol{u}_h^n, \nabla\cdot\boldsymbol{v}_h\rangle - \langle \alpha p_h^n, \nabla\cdot\boldsymbol{v}_h\rangle + \langle \alpha\nabla\cdot\boldsymbol{u}_h^n, q_h\rangle \\ = \left\langle \frac{1}{M}p_h^{n-1}, q_h\right\rangle + \Delta t\langle S_f, q_h\rangle + \langle \alpha\nabla\cdot\boldsymbol{u}_h^{n-1}, q_h\rangle + \langle \boldsymbol{f}, \boldsymbol{v}_h\rangle\ .\end{aligned}$$

Step 2: Find $c_h^{n,i} \in B_h$ given $\boldsymbol{w}_h^n \in \boldsymbol{Z}_h$, $c_h^{n,i-1} \in B_h, c_h^{n-1} \in B_h$ such that for all $b_h \in B_h$ there holds

$$\begin{aligned}\langle c_h^{n,i}, b_h\rangle + \Delta t\langle D\nabla c_h^{n,i}, \nabla b_h\rangle + \Delta t\langle \nabla c_h^{n,i}\cdot\boldsymbol{w}_h^n, b_h\rangle + \Delta t\langle c_h^{n,i}\nabla\cdot\boldsymbol{w}_h^n, b_h\rangle + \langle L_2 c_h^{n,i}, b_h\rangle = \\ \Delta t\langle S_c, b_h\rangle + \Delta t\langle R(c_h^{n,i-1}), b_h\rangle + \langle c_h^{n-1}, b_h\rangle + \langle L_2 c_h^{n,i-1}, b_h\rangle\ .\end{aligned}$$

Case 2

In this case, both the Biot equations and the transport equation are solved in a monolithic manner. This is done by first solving the Biot equations monolithically, and then use the Darcy flux approximated in the fully coupled Biot equations as the flow field in the transport equation. The stopping criterion for this iterative process is the same as the one used for the fixed stress splitting method.

This procedure consists of two steps which reads as follows:
Step 1: Find $(p_h^{n,i}, \boldsymbol{w}_h^{n,i}, \boldsymbol{u}_h^{n,i}) \in Q_h \times \boldsymbol{Z}_h \times \boldsymbol{V}_h$ given $(p_h^{n,i-1}, \boldsymbol{w}_h^{n,i-1}, \boldsymbol{u}_h^{n,i-1}) \in Q_h \times \boldsymbol{Z}_h \times \boldsymbol{V}_h$ and $(p_h^{n-1}, \boldsymbol{w}_h^{n-1}, \boldsymbol{u}_h^{n-1}) \in Q_h \times \boldsymbol{Z}_h \times \boldsymbol{V}_h$ such that for all $(q_h, \boldsymbol{z}_h, \boldsymbol{v}_h) \in Q_h \times \boldsymbol{Z}_h \times \boldsymbol{V}_h$ there holds

$$\begin{aligned}\langle \boldsymbol{K}^{-1}\boldsymbol{w}_h^{n,i}, \boldsymbol{z}_h\rangle - \langle p_h^{n,i}, \nabla\cdot\boldsymbol{z}_h\rangle + \left\langle \frac{1}{M}p_h^{n,i}, q_h\right\rangle + \Delta t\ \langle \nabla\cdot\boldsymbol{w}_h^{n,i}, q_h\rangle + \langle 2\mu\varepsilon(\boldsymbol{u}_h^{n,i}), \varepsilon(\boldsymbol{v}_h)\rangle \\ + \langle \lambda\nabla\cdot\boldsymbol{u}_h^{n,i}, \nabla\cdot\boldsymbol{v}_h\rangle - \langle \alpha p_h^{n,i}, \nabla\cdot\boldsymbol{v}_h\rangle + \langle \alpha\nabla\cdot\boldsymbol{u}_h^{n,i}, q_h\rangle \\ = \left\langle \frac{1}{M}p_h^{n-1}, q_h\right\rangle + \Delta t\langle S_f, q_h\rangle + \langle \alpha\nabla\cdot\boldsymbol{u}_h^{n-1}, q_h\rangle + \langle \boldsymbol{f}, \boldsymbol{v}_h\rangle\ .\end{aligned}$$

Step 2: Find $c_h^{n,i} \in B_h$ given $\boldsymbol{w}_h^{n,i} \in \boldsymbol{Z}_h$, $c_h^{n,i-1} \in B_h, c_h^{n-1} \in B_h$ such that for all

$b_h \in B_h$ there holds

$$\langle c_h^{n,i}, b_h\rangle + \Delta t\langle D\nabla c_h^{n,i}, \nabla b_h\rangle + \Delta t\langle \nabla c_h^{n,i}\cdot \boldsymbol{w}_h^{n,i}, b_h\rangle + \Delta t\langle c_h^{n,i}\nabla\cdot \boldsymbol{w}_h^{n,i}, b_h\rangle + \langle L_2 c_h^{n,i}, b_h\rangle = \Delta t\langle S_c, b_h\rangle + \Delta t\langle R(c_h^{n,i-1}), b_h\rangle + \langle c_h^{n-1}, b_h\rangle + \langle L_2 c_h^{n,i-1}, b_h\rangle \ .$$

The efficiency of the different methods in the unit square are plotted in Figure 4.7. We have studied the difference in elapsed time between the fixed stress splitting scheme with the optimal tuning parameter $L = \frac{\alpha^2}{2\left(\frac{2\mu}{d}+\lambda\right)}$, Case 1, where the Biot equations are solved monolithically and the transport equation iteratively, and Case 2, where both the Biot equations and the transport equation is solved monolithically. The computations were performed on a MacBook Air with a 1.6 GHz Intel Core i5 processor. For a more realistic plot of the efficiency for the unit square, we increase the number of refinements of the mesh to five, and accordingly the final space step size is $h = 0.015625$.

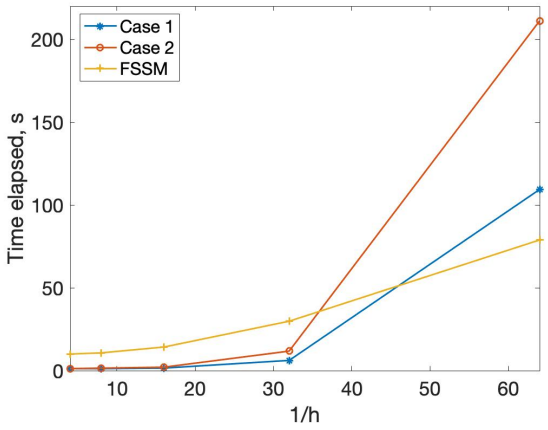

Figure 4.7: Time elapsed after computing the system for different mesh sizes in the unit square.

By studying this plot, we notice the rapid increase in time elapsed when refining the mesh from a 32x32 mesh to a 64x64 mesh for Case 2. Case 1, with monolithically solved Biot equations and iteratively solved transport equation, also increases quite fast when refining the mesh in this interval. The fixed stress splitting method has only a slight increase in the same interval, and is consequently the fastest method for the 64x64 mesh.

We now consider the L-shaped domain. The efficiency for this domain is plotted in Figure 4.8, and the schemes we study are the same as for the unit square.

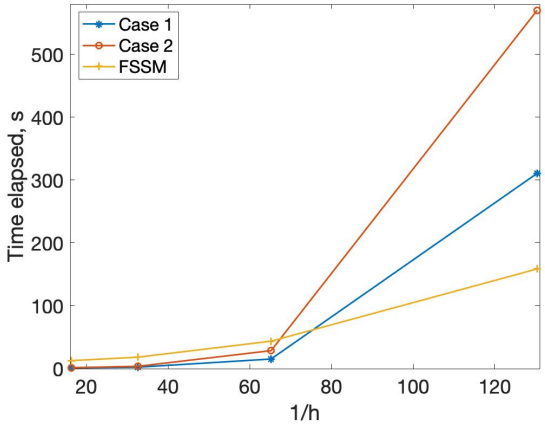

Figure 4.8: Time elapsed after computing the system for different mesh sizes in the L-shaped domain.

Please note that the step sizes are smaller than for the unit square, hence the number of unknowns are greater for the L-shaped domain and consequently the time elapsed is longer. In this plot as well, the fixed stress splitting method appears to be the best method for solving our system. The method is much faster than Case 1 and Case 2 for the finest mesh we tested, though slightly slower than the other methods for the coarser meshes.

After studying both Figure 4.7 and Figure 4.8, our conclusion is that for finer meshes, the fixed stress splitting method is the most efficient method for our system of equations. However, as we observe that there is only a slight difference in the time elapsed for the different methods when h is large, the choice of method is of little consequence for the coarser meshes.

4.2 Convergence studies

We will now observe the convergence rate, that is how fast the error approaches zero when the resolution is increased. The L^2-norm of the error is obtained by taking the L^2-norm of the approximated solutions at the final time minus the associated

exact solutions, $\|e_h\| = \|(\boldsymbol{u}_h, p_h, \boldsymbol{w}_h, c_h) - (\boldsymbol{u}, p, \boldsymbol{w}, c)\|$. If this error is bounded by the space step size h to some power p, and the approximated solution goes to the exact solution when $h \to 0$, the method converges. To find how fast the approximated solution goes to the exact solution, we can observe the convergence rate p in $\|e_h\| \leq Ch^p$, where C is some constant. This is done by replacing "$\leq$" with "$=$" and using logarithms. The convergence rate is then obtained by computing

$$p = \frac{\log\left(\frac{\|e_{h_2}\|}{\|e_{h_1}\|}\right)}{\log\left(\frac{h_2}{h_1}\right)} ,$$

where e_{h_1} and e_{h_2} are the errors at the last time step for two different space step sizes, h_1 and h_2.

Looking at the approximation spaces 3.4, 3.5, 3.6, 3.10, we see from the functions in each triangle that the convergence rates should be 1 for the flux and pressure, and 2 for the displacement and concentration. This means that the flux and pressure converges linearly, while the displacement and concentration converges quadratically (Knabner and Angermann, 2003). When computing the convergence rates for the flux, pressure, displacement and concentration in accordance with the previously mentioned method, we see that this is indeed the case for our problem. In the following plots we have drawn a line with that corresponding slope for reference, 1 for flux and pressure, and 2 for displacement and concentration.

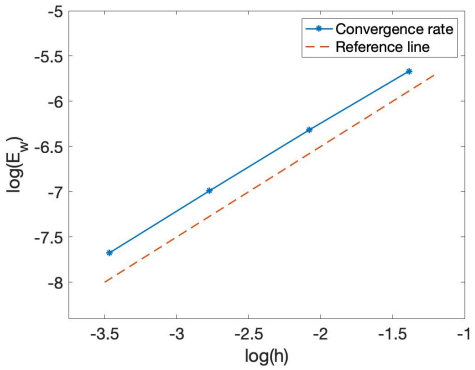

(a) Error in flux, the reference line has a slope of 1.

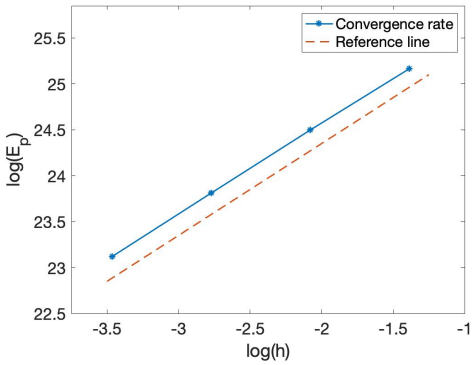

(b) Error in pressure, the reference line has a slope of 1.

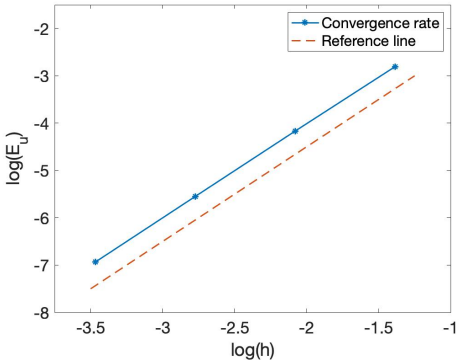

(c) Error in displacement, the reference line has a slope of 2.

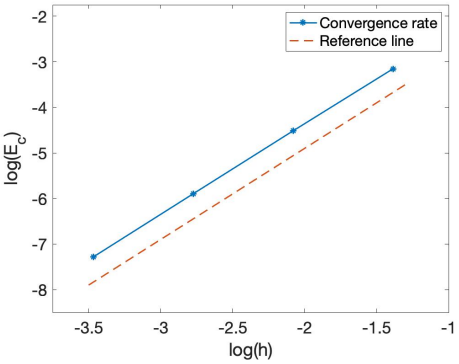

(d) Error in concentration, the reference line has a slope of 2.

Figure 4.9: Plots of error and step size in the unit square. Please notice the difference in the axes.

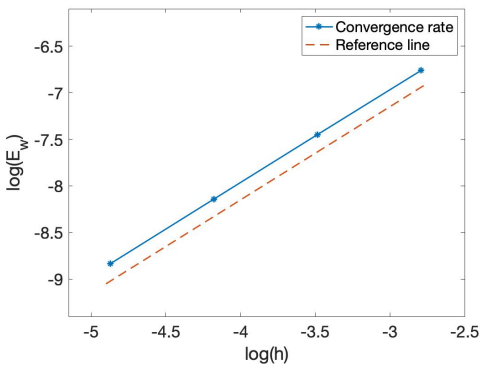

(a) Error in flux, the reference line has a slope of 1.

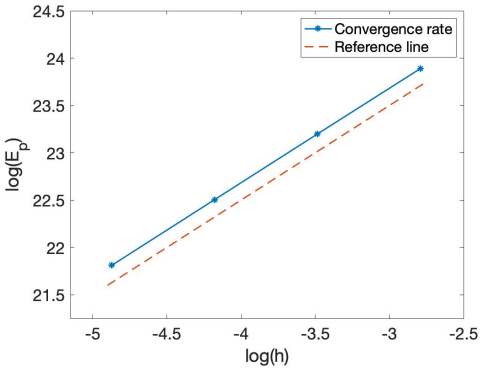

(b) Error in pressure, the reference line has a slope of 1.

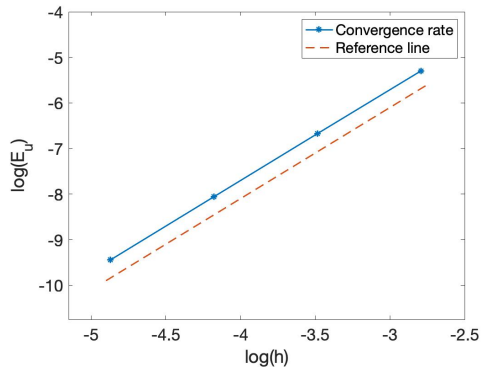

(c) Error in displacement, the reference line has a slope of 2.

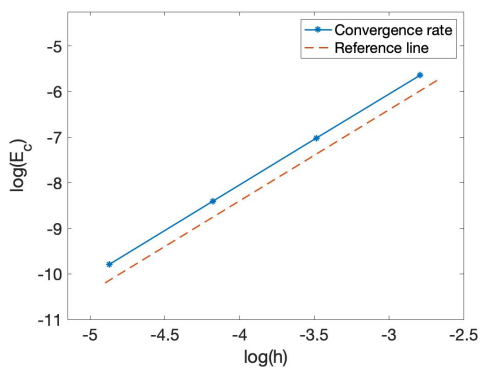

(d) Error in concentration, the reference line has a slope of 2.

Figure 4.10: Plots of error and step size in the L-shaped domain. Please notice the difference in the axes.

These plots demonstrate clearly that the convergence rates are correct in accordance with the approximation spaces, which implies that our proposed iterative solution scheme for solving the Biot model coupled with a transport equation is performing robustly and efficiently.

Chapter 5

Conclusions & Future Work

5.1 Conclusions

In this thesis, the quasi-static Biot equations, which models flow and mechanics in a linearly elastic deformable porous media, have been coupled one-way with a transport equation and studied numerically. The fixed stress splitting method has been adapted to fit this situation and has been tested on a test problem. Three different tuning parameters were proposed, and we found that the optimal choice was $L = \frac{\alpha^2}{2\left(\frac{2\mu}{d}+\lambda\right)}$. Furthermore, four different reaction terms were studied for the transport equation. They were all convergent. The stabilizing parameter, introduced by linearizing the reaction term, has been studied, and we found that our scheme was not sensitive to the choice of this parameter. Moreover, two domains were studied, the unit square and the L-shaped domain, and the results were the same on both.

Following this, we compared the efficiency of the fixed stress splitting scheme with the efficiency of two different monolithic schemes. One where the Biot equations are solved monolithically, and the transport equation is solved iteratively, and one where both are solved monolithically. The result was that the fixed stress splitting scheme was the most efficient scheme for finer meshes, while for coarser meshes, the choice of method was of little consequence.

Convergence tests on the problem gave the expected convergence rates in both domains, thus we can conclude that the method works well for a one-way coupling

between the quasi-static Biot equations and the nonlinear transport equation in two dimensions. To the best of our knowledge, the coupling between the transport equation and the quasi-static Biot equations has not been reported in literature yet. Even though we only tested the scheme on a test problem, this work has showed that the Biot equations and the nonlinear transport equation can be coupled and solved iteratively using the proposed methodology, and yields satisfying results.

5.2 Future work

We suggest extending the model to three dimensions to be able to create a more realistic model that can be applied to a realistic tumor problem. For further testing of the coupling connection between the Biot equations and the transport equation, it is necessary to implement a realistic problem, for example the Mandel's problem, in order to compare the numerical results with the experimental results. Additionally, a two-way coupling of the Biot equations and transport equation should be implemented and tested. A validation of the model assumptions should also be performed. We observe that the stabilization term in the transport equation does not affect the number of iterations. To get a precise understanding of this phenomenon, additional analysis is needed. Furthermore, a theoretical analysis of the convergence of the scheme should be performed to further validate the coupling of the Biot model with reactive transport.

Bibliography

Almani, T., Kumar, K., Dogru, A., Singh, G., and Wheeler, M. (2016). Convergence analysis of multirate fixed-stress split iterative schemes for coupling flow with geomechanics. *Computer Methods in Applied Mechanics and Engineering*, 311:180–207.

Bahriawati, C. and Carstensen, C. (2005). Three matlab implementations of the lowest-order raviart-thomas mfem with a posteriori error control. *Computational Methods in Applied Mathematics*, 5:333–361.

Bause, M., Radu, F., and Köcher, U. (2017). Space-time finite element approximation of the biot poroelasticity system with iterative coupling. *Computer Methods in Applied Mechanics and Engineering*, 320:745–768.

Bear, J. (1988). *Dynamics of Fluids in Porous Media*. NY: Dover.

Biot, M. A. (1941). General theory of three-dimensional consolidation. *Journal of Applied Physics*, 12(2):155–164.

Biot, M. A. (1955). Theory of elasticity and consolidation for a porous anisotropic solid. *Journal of Applied Physics*, 26(2):182–185.

Borregales, M., Kumar, K., Radu, F. A., Rodrigo, C., and Gaspar, F. J. (2019). A partially parallel-in-time fixed-stress splitting method for biot's consolidation model. *Computers & Mathematics with Applications*, 77(6):1466–1478.

Borregales, M., Radu, F., Kumar, K., and M. Nordbotten, J. (2018). Robust iterative schemes for non-linear poromechanics. *Computational Geosciences*, 22:1021–1038.

Both, J., Borregales, M., Nordbotten, J., Kumar, K., and Radu, F. (2017). Ro-

bust fixed stress splitting for biot's equations in heterogeneous media. *Applied Mathematics Letters*, 68:101–108.

Both, J., Kumar, K., Martin Nordbotten, J., and Radu, F. (2019). Anderson accelerated fixed-stress splitting schemes for consolidation of unsaturated porous media. *Computers & Mathematics with Applications*, 77:1479–1502.

Braess, D. (2007). *Finite Elements: Theory, Fast Solvers, and Applications in Solid Mechanics*. Cambridge University Press, 3rd edition.

Brun, M., Elyes, A., Berre, I., Martin Nordbotten, J., and Radu, F. (2019). Monolithic and splitting based solution schemes for fully coupled quasi-static thermo-poroelasticity with nonlinear convective transport. arXiv:1902.05783.

Cheney, W. (2001). *Analysis for Applied Mathematics*. Springer.

Coussy, O. (2004). *Poromechanics*. John Wiley & Sons.

Dullien, F. A. L. (1979). *Porous Media Fluid Transport and Pore Structure*. Academic Press, 1st edition.

Dyke, T. J. V. and Hoger, A. (2000). A comparison of second-order constitutive theories for hyperelastic materials. *International Journal of Solids and Structures*, 37(41):5873–5917.

Iserles, A. (2008). *A First Course in the Numerical Analysis of Differential Equations*. Cambridge Texts in Applied Mathematics. Cambridge University Press, 2nd edition.

Johnson, C. (1987). *Numerical solution of partial differential equations by the finite element method*. Studentlitteratur, Lund.

Kim, J., Tchelepi, H., and Juanes, R. (2009). Stability, accuracy and efficiency of sequential methods for coupled flow and geomechanics. *SPE Journal*, 16:249–262.

Kim, J., Tchelepi, H., and Juanes, R. (2011). Stability and convergence of sequential methods for coupled flow and geomechanics: Fixed-stress and fixed-strain splits. *Computer Methods in Applied Mechanics and Engineering*, 200(13):1591–1606.

Knabner, P. and Angermann, L. (2003). *Numerical Methods for Elliptic and*

Parabolic Partial Differential Equations. Number Vol. 44 in Texts in Applied Mathematics. Springer.

Langtangen, H. P. and Logg, A. (2017). *Solving PDEs in Python: The FEniCS Tutorial I.* Springer Publishing Company, Incorporated, 1st edition.

List, F. and Radu, F. A. (2016). A study on iterative methods for solving richards' equation. *Computational Geosciences*, 20(2):341–353.

Logg, A., Mardal, K.-A., Wells, G. N., et al. (2012). *Automated Solution of Differential Equations by the Finite Element Method.* Springer.

Mikelić, A., Wang, B., and Wheeler, M. F. (2014). Numerical convergence study of iterative coupling for coupled flow and geomechanics. *Computational Geosciences*, 18(3):325–341.

Mikelić, A. and Wheeler, M. F. (2013). Convergence of iterative coupling for coupled flow and geomechanics. *Computational Geosciences*, 17(3):455–461.

Nordbotten, J. and Celia, M. (2011). *Geological Storage of CO2: Modeling Approaches for Large-Scale Simulation.* John Wiley & Sons.

Pettersen, Ø. (1990). Grunnkurs i reservoarmekanikk.

Settari, A. and Mourits, F. M. (1998). A coupled reservoir and geomechanical simulation system. *SPE Journal*, 3:219–226.

Showalter, R. (2000). Diffusion in poro-elastic media. *Journal of Mathematical Analysis and Applications*, 251(1):310–340.

Storvik, E., Both, J., Kumar, K., Martin Nordbotten, J., and Radu, F. (2018). On the optimization of the fixed-stress splitting for biot's equations. arXiv:1811.06242v2.

Xue, S.-L., Li, B., Feng, X.-Q., and Gao, H. (2016). Biochemomechanical poroelastic theory of avascular tumor growth. *Journal of the Mechanics and Physics of Solids*, 94:409–432.